

2017

Indoor Localization Based on Visible Light Communication

Yi Wang
Lehigh University

Follow this and additional works at: <http://preserve.lehigh.edu/etd>



Part of the [Electrical and Computer Engineering Commons](#)

Recommended Citation

Wang, Yi, "Indoor Localization Based on Visible Light Communication" (2017). *Theses and Dissertations*. 2869.
<http://preserve.lehigh.edu/etd/2869>

This Thesis is brought to you for free and open access by Lehigh Preserve. It has been accepted for inclusion in Theses and Dissertations by an authorized administrator of Lehigh Preserve. For more information, please contact preserve@lehigh.edu.

Indoor Localization Based on Visible Light Communication

By

Yi Wang

A Thesis

Presented to the Graduate and Research Committee

of Lehigh University

in Candidacy for the Degree of

Master of Science

in

Electrical Engineering

Lehigh University

May, 2017

THESIS SIGNATURE SHEET

This thesis is accepted and approved in partial fulfillment of the requirements for the Master of Science.

May 5, 2017

Date

Jing Li

Thesis Advisor

Co-Advisor

Svetlana Tatic-Lucic

Department Chair

Contents

List of Figures.....	v
List of Tables.....	vi
Abstract.....	1
1 Introduction.....	3
1.1 Indoor Localization Based on Visible Light Communication.....	3
1.2 Visible Light.....	5
1.3 Optical Source – Light-emitting Diode.....	7
1.4 Photodetectors and Photodetection Techniques.....	9
1.4.1 Photodetectors.....	9
1.4.2 Photodetection Schemes.....	11
2 Modeling of Indoor VLC Channel.....	14
2.1 Configuration of VLC Link.....	15
2.2 Model of Directed LOS Optical Channel.....	17
2.3 Model of Nondirected LOS Optical Channel.....	18
2.4. Signal-to-noise Ratio Analysis.....	20
2.5 Discussion on Electrical SNR.....	23
2.6 Conclusion.....	24
3 Indoor Localization Based on VLC.....	25
3.1 VLC System using IM/DD.....	25
3.2 Localization Methods for VLC Based Indoor Localization.....	26
3.3 Dilution of Precision Analysis for RSS-based Localization using VLC.....	30

3.3.1 Formulation of Measurement Equation.....	30
3.3.2 DOP for RSS-Based Localization	32
3.3.3 Simulation Results.....	35
4 Conclusion and Future Work.....	39
References	41

List of Figures

Figure 1.1: Electromagnetic spectrum.....	7
Figure 1.2: Diagram of an IM/DD optical receiver.....	12
Figure 1.3: Diagram of a coherent photodetection optical receiver.....	12
Figure 2.1: Link configurations.....	16
Figure 2.2: The first reflection of the nondirected LOS optical link.....	20
Figure 2.3: Distribution of received optical power with reflection.....	20
Figure 3.1: Illustrative diagram of VLC system using IM/DD.....	26
Figure 3.2: Channel model of VLC system using IM/DD.....	26
Figure 3.3: Localization based on TOA methods.....	27
Figure 3.4: Localization based on RSS methods.....	29
Figure 3.5: Localization based on AOA methods.....	29
Figure 3.6: Indoor localization scenario 1.....	36
Figure 3.7: Indoor localization scenario 2.....	36
Figure 3.8: Positioning nodes in scenario 1.....	37
Figure 3.9: Positioning nodes in scenario 2.....	37
Figure 3.10: PDOP surface for scenario 1.....	37
Figure 3.11: PDOP surface for scenario 2.....	37

List of Tables

Table 2.1: Approximate spectral colors of visible light.	6
Table 3.1: Simulation parameters for LED and photo-detector	36
Table 3.2: PDOP value for RSS-based localization	37
Table 3.3: Positions with maximum and minimum PDOP	38

Abstract

With the increasing demand for accurate indoor localization and widespread deployment of light-emitting diodes (LEDs) for lighting, there has been a dramatic rise in research activities in many areas of indoor localization based on visible light communication (VLC), including modeling of VLC channels, localization methods, localization algorithms, and localization systems.

In VLC based indoor localization systems, the reflection, interference and noise in the VLC channels cause the loss, fading and distortion of the transmitted signals. The bandwidth and the signal-to-noise ratio (SNR) of the channel directly affect the channel capacity, the design of modulation scheme, the transmitted power and the data rate. Therefore, it is imperative to capture the characteristics of different VLC channels and properly model them for dual purpose of illumination and localization. We start by a systematic investigation of the VLC channel models. We first investigate three possible configurations of indoor VLC links, and evaluate two widely used VLC channel models – the directed light-of-sight (LOS) optical channel and the nondirected LOS optical channel model. We next investigate the electrical SNR for VLC channels with intersymbol interference (ISI) and without ISI, and provide closed-form derivations to clarify some confusion on the electrical SNR in the literature.

To help design and especially evaluate VLC localization schemes, we investigate, analyze and compare four possible localization methods applied to indoor VLC

localization – time of arrival (TOA) methods, time difference of arrival (TDOA) methods, received signal strength (RSS) methods and angle of arrival (AOA) methods. For practicality, we consider intensity modulation and direct detection (IM/DD) and explore the dilution of precision (DOP) analysis, a metric that has been successfully deployed in GPS localization and AOA-based localization. For RSS-based indoor VLC localization, we establish a closed-form relation between positional DOP (PDOP) and the accuracy of RSS-based indoor VLC localization, use PDOP to analyze two localization scenarios with different LED grid patterns, and quantize the effect of LED grid patterns on the position errors. Simulation results confirm the effectiveness of the proposed approach.

Chapter 1

Introduction

1.1 Indoor Localization Based on Visible Light Communication

There is an increasing demand for accurate indoor localization technologies and location-based applications for indoor areas. Indoor localization could provide surveillance, navigation and object tracking services, which have broad and important applications in many areas, such as warehouses, indoor parking facilities, museums and supermarkets. Although the global positioning system (GPS) works well for outdoor localization, it is difficult to apply GPS signals to indoor localization, because the drastic attenuation of GPS signals through building walls and multipath propagation in the indoor environment will result in uncontrollable errors. Previously, several other technologies, such as ultrasound [1] and radio waves [2][3][4], have been explored for indoor localization. Each has its drawbacks that limit its ubiquitous applications. The wavelength of ultrasound is relatively large, and its velocity is affected by environment temperature, which may result in large ranging and localization errors. The difficulties of radio frequency (RF) based localization lie in the multipath effect of radio signals in the indoor environment, electromagnetic (EM) radiation, and very limited RF spectrum resources. The multipath effect increases localization errors, and the EM radiation limits the application of RF based localization in RF sensitive environments such as hospitals and airplanes.

With soon-to-be ubiquity of light-emitting diodes (LEDs), indoor localization based on visible light communication (VLC) is gaining tremendous research attention. Generally, VLC based indoor localization makes full use of the data transmitted by VLC and the information measured from visible light signals for localization. These data and information include positions of LEDs, positions of other anchors, time stamps, incident angles, and arrival angles etc. VLC based indoor localization has two unique advantages. The multipath effect of optical signals in the indoor environment is much less than RF signals, because the reflected optical signals typically have much lower power than the light-of-sight (LOS) signal [4], which provides potentially high localization accuracy. Further, the radio frequency (RF) spectrum is increasingly congested and sparse, but the available optical spectrum of VLC is considerably broad.

However, there are still many challenges which need to be addressed in the topic. The VLC channel models for different indoor environments are still not precisely. Some previous articles and review papers in this topic didn't address the issue of the channel models clearly, and had some confusing definitions, equations and deductions. In addition, different configuration schemes for indoor localization result in difficulties to compare and evaluate their localization errors, and there is still lack of good and general criteria to evaluate the localization errors for VLC based indoor localization.

This research is dedicated to the study of indoor localization based on VLC. Specific focus will be set on the investigation and analysis of indoor VLC channel models, the

analysis and deduction of the electrical SNR, and the dilution of precision (DOP) analysis for RSS-based localization using VLC. The first chapter investigates visible light, LEDs, photodetectors and photodetection techniques. The second chapter approaches the channel models in a relatively systematic manner. This chapter mainly focuses on the investigation of two widely used VLC channel models, analysis of the electrical SNR, provide closed-form derivations to clarify some confusion on electrical SNR in the literature. The third chapter investigate, analyze and compare four possible localization methods applied in VLC based indoor localization, and explore the DOP analysis for evaluating the localization accuracy of RSS-based indoor localization using VLC. The DOP relates the localization error to the measurement error, which is used for GPS localization and AOA-based localization. However, few works have been found to focus on DOP analysis for RSS-based localization using VLC. We establish the relation between positional DOP (PDOP) and localization errors for RSS-based indoor localization using VLC, then use PDOP to analyze two localization scenarios with different of LED grid patterns, quantize the effect of LED grid patterns on the position error of the mobile receiver. Simulation results confirm our approach.

1.2 Visible Light

Visible light is a portion of the EM spectrum that the human eyes are the most sensitive to. In nature, the visible light most commonly seen comes from the sunlight. Although sunlight covers other lights beyond the visible region, its peak power is mainly in the visible region [5]. From the view of EM spectrum, the visible spectrum extends from

about 390 to 700 nm in terms of wavelength, and 430 to 770 THz in terms of frequency [5]. Fig. 1.1 shows the EM spectrum [6]. The EM spectrum ranges from long waves with very low frequency to gamma rays with high frequency, and therefore covers wavelengths ranging from several kilometers for long waves down to the size less than an atom for gamma rays. From Fig. 1.1, we can see that visible light is just a small portion of the whole EM spectrum. Another way to view visible light is the colors it produces. The colors that can be generated by visible light within different and narrow frequency band are called pure spectral colors. Table 1.1 shows the approximate spectral colors of visible light [6].

Color	Wavelength	Frequency
violet	380–450 nm	668–789 THz
blue	450–495 nm	606–668 THz
green	495–570 nm	526–606 THz
yellow	570–590 nm	508–526 THz
orange	590–620 nm	484–508 THz
red	620–750 nm	400–484 THz

Table 1.1: Approximate spectral colors of visible light [6].

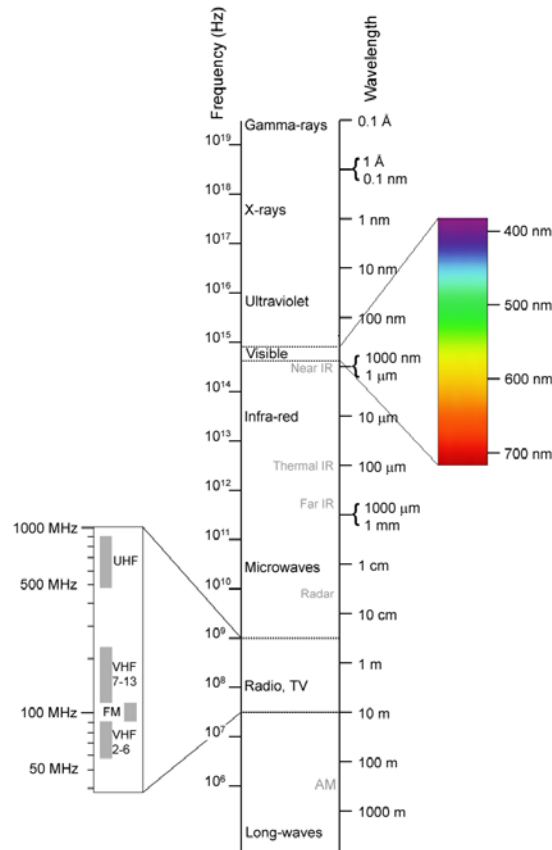


Figure 1.1: Electromagnetic spectrum [6].

1.3 Optical Source – Light-emitting Diode

The LED is a kind of solid-state lighting source, which generates light through solid-state electroluminescence. LEDs can be manufactured to generate light across a wide range of wavelengths, ranging from the visible light to the infrared ray (IR). The research and application of LEDs have a relatively short history. Back in the 1990s, the LEDs were just introduced for the application of general illumination. However, during the past few years, researchers and engineers have improved LED's luminous efficiency rapidly from less than 0.1 lm/W to over 260 lm/W [7][8]. And the lifetime of the LED is also improved rapidly.

The core part of the LED is a semiconductor p–n junction. When a forward bias voltage is applied on the p–n junction, this p–n junction is excited and generates optical radiation spontaneously. This process is called as electronic excitation. This electronic excitation energizes electrons in the semiconductor material into an excited state. The excited state is unstable. Then the energized electrons return to the stable state, and give off photons spontaneously. For the radiative recombination, the electronic excitation causes the excited electrons in the conduction band of semiconductor material to return to its valence band. The energy of the emitted photons is equal to the band-gap energy, that is, the energy difference between the conduction band and the valence band. The optical radiation of the LED could be ultraviolet (UV), visible or infrared depending on the energy band-gap of the semiconductor material. In the case of radiative recombination process, the luminescence intensity of optical radiation and its energy are given by [9]

$$I = I(E) \propto \sqrt{E - E_g} \exp\left(-\frac{E}{kT}\right) \quad (1.1)$$

$$E = hf = \frac{hc}{\lambda} \quad (1.2)$$

where I is luminescence intensity, E is the energy of photons, E_g is the band-gap energy of the semiconductor material, k is the Boltzmann constant and T is the absolute temperature, h is Planck constant, f is the frequency of radiation, c is the speed of light, and λ is the wavelength of radiation.

Based on the above analysis, we can see that the optical power radiated by the LED depends significantly on the band-gap energy of the semiconductor materials of the p–n

junction. In addition, the optical power radiated by the LED is proportional the driving current passing through its p–n junction. As the driving current is increased, the optical power also increases [10]. For more comprehensive elaboration, analysis and discussion of the principle, structure and applications of the LED, please refer to related books [9][11].

The LEDs have a number of prominent advantages. Compared with traditional lights such as fluorescent lights with a luminous efficiency limited to 90 lm/W and incandescent lights with a luminous efficiency limited to 52 lm/W, the white LEDs can reach very high luminous efficiency (energy conversion efficiency) with the peak efficiency exceeding 260 lm/W [7][8]. Other advantages include but are not limited to longer lifetime, fast switching, mercury free, lower power consumption and less heat generation [7][12]. Due to these advantages, the LEDs are not only ideal lighting sources for contributing to considerable energy savings, but also ideal transmitters for indoor localization and data communications.

1.4 Photodetectors and Photodetection Techniques

1.4.1 Photodetectors

The photodetector is a kind of optoelectronic transducer which can convert the instantaneous inputted optical signal to electrical current. Generally, the electrical current outputted by a photodetector is proportional to the instantaneous optical power it receives.

If an incident optical signal with an average power P_r impinges on a photodetector over a period of time, then the average electrical current generated by the photodetector is given by [13]

$$\langle i \rangle = \frac{\eta_{qe} q \lambda P_r}{hc} = R P_r \quad (1.3)$$

where q is the electronic charge, λ is the wavelength of the incident optical radiation, η_{qe} is the quantum efficiency, and R is the photodetector responsivity. R is defined as the photocurrent generated per unit incident optical power, which is given by

$$R = \frac{\eta_{qe} q \lambda}{hc} \approx \frac{\eta_{qe} q \lambda}{1.24} \quad (1.4)$$

Since the optical signals transmitted by the light source travel through complex communication channel and experience loss, fading and distortion, the optical signals received by the photodetector are usually weak. In order to collect as much optical power as possible and meanwhile reduce the interference of background light and noise, the photodetector used for VLC should meet some requirements such as large detection surface area, high sensitivity and responsivity within its operational range of wavelengths, a low noise level and an adequate receiving bandwidth for the desired data transmission rate [10]. Currently, there are several types of photodetectors that can be used for receiving optical radiations. Among them, the most widely used for optical wireless communication, including VLC, are PIN photodetector and avalanche photodiode (APD) photodetectors.

1.4.2 Photodetection Schemes

The aim of photodetection is to recover the information modulated on the transmitted optical signals from the received signals. Usually, the information can be modulated on the frequency, phase or the intensity of the transmitted optical signals. Currently, two photodetection techniques are applied in optical wireless communications including intensity-modulation and direct detection (IM/DD) and coherent detection. Currently, due to the inconsistent phase of light radiated from the LED, the IM/DD scheme is widely in VLC system.

In the IM/DD scheme, only the intensity of the optical signal radiated from an LED is modulated to convey the information. The transmitted information is related to the variation of the intensity of the transmitted optical radiation. IM/DD is also known as the envelope detection, and therefore a local oscillator is not needed in the detection process. The IM/DD is a very simple detection scheme and therefore is widely adopted in optical receiver. The disadvantage of this scheme is that it only uses intensity of the optical signal which just has one degree of freedom. Figure 1.2 shows the basic diagram of an IM/DD optical receiver [10]. In IM/DD scheme, for the input optical radiation with the instantaneous incident power $P(t)$, the instantaneous photodetector current $i(t)$ generated by photodetector is given by

$$i(t) = \frac{\eta_{qe} q \lambda}{hc} MP(t) \quad (1.5)$$

where M is the gain of photodetector in the optical receiver, and the other parameters are same as those defined in (1.4).

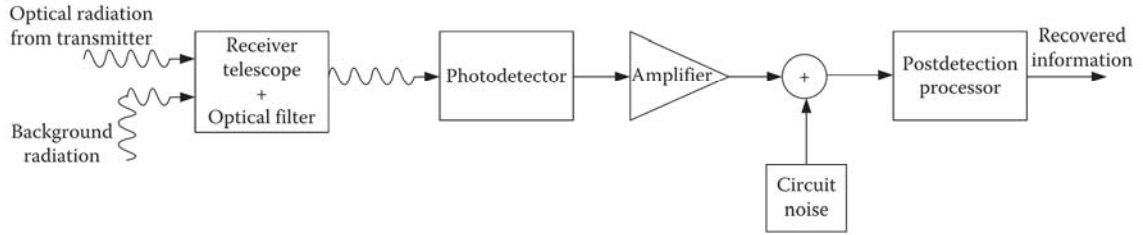


Figure 1.2: Diagram of an IM/DD optical receiver [10].

In the coherent photodetection scheme, the amplitude, phase and frequency of the optical signal can be modulated to convey the information. In the receiver, an optical local oscillator (OLO) is applied for demodulation. Through combining the optical signal generated by OLO with the received optical signal, the receiver performs demodulation and further restores the information including amplitude, phase and frequency on transmitted optical signals. However, the disadvantage of coherent photodetection scheme is that optical receivers for this scheme are sensitive to the phase and the state of polarization of the received optical signal. Figure 1.3 shows the basic block diagram of coherent photodetection optical receiver [10].

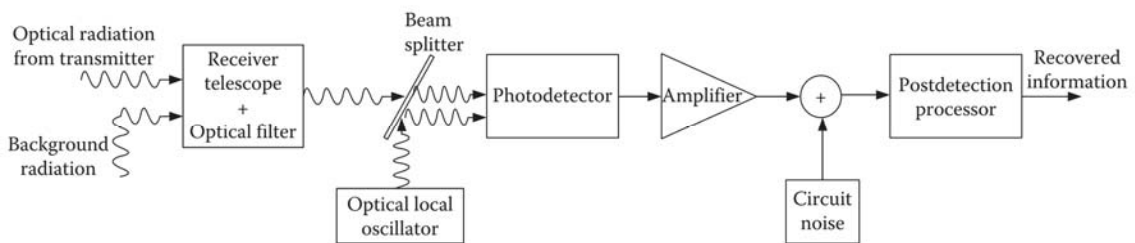


Figure 1.3: Diagram of a coherent photodetection optical receiver [10].

Unlike RF coherent detection, the output signal of OLO in optical coherent detection doesn't necessarily have the same frequency or phase as the received optical signal.

There are two types of optical coherent detection. One is heterodyne detection, and the other is homodyne detection. In heterodyne detection, the frequency of the optical signal generated by OLO is about several gigahertz different from the frequency of the received optical signal. However, in the homodyne detection, the frequency and phase of the optical signal generated by OLO should be same as the received optical signal. The advantage of homodyne detection is that the modulated received optical signal can be directly demodulated to the baseband signal for further processing [14].

Chapter 2

Modeling of Indoor VLC Channel

In both VLC based indoor localization systems and VLC systems, the optical signals emitted from the LED travel through the complex communication channel. Due to some negative characteristics of the VLC channels such as reflection, diffusion, interference and noise, the channel causes the loss, fading and distortion of the transmitted signal. In addition, the bandwidth and SNR of the channel directly affect the channel capacity, the design of modulation scheme, the transmitted power, and the data transmission rate. The channel of VLC has specific features, which are quite different from the channels of wireless communication. Therefore, it is very important to well understand of the characteristics of different channels of VLC, and establish suitable models for those channels.

However, some previous articles and review papers in this topic didn't address the issue of channel models clearly, and had some confusing definitions, equations and deductions [12][16]. In this chapter, we approach the channel models in a relatively systematic manner. We first investigate three possible configuration schemes of VLC links, and investigate the directed LOS optical channel model and the nondirected LOS optical channel. Then we analyze the electrical SNR, analyze the effect of detector area on the electrical SNR and receiving bandwidth, and derive some useful results. Finally, we clarify some confusion in the related paper through analysis and deduction.

2.1 Configuration of VLC Link

In a typical room environment, visible light signal will be reflected by walls, the ceiling, and the surfaces of some other objects such as furniture and appliances in the room. Currently, there are several ways to configure visible light communication links in a typical room. This section briefly investigates three commonly applied configurations in VLC and localization based VLC: directed LOS, nondirected LOS and diffuse configuration. For more details about these configurations, please refer to other related references [17][18].

In the directed LOS configuration, a point-to-point communication link should be built directly between the transmitter and the optical receiver, as shown in Fig 2.1 (a). This configuration doesn't suffer from multipath signal distortion caused by reflections, and can largely reduce the interference induced by ambient light from other light sources. Also, it requires low optical power for the transmitter, but can offer the highest data rate given the same transmitted power and the same distance between the transmitter and receiver. However, the disadvantage of LOS configuration is also obvious. The coverage area of the optical signal is very small, and it is not easy to precisely align the receiver and transmitter.

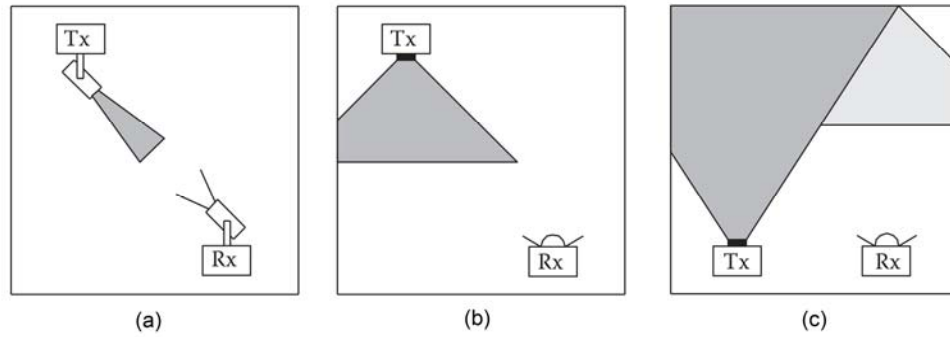


Figure 2.1: Link configurations: (a) Directed LOS, (b) Nondirected LOS, (c) Diffuse, where Tx represents the transmitter and Rx represents the receiver [10].

Nondirected LOS configuration consists of wide beam transmitters, wide field-of-view (FOV) optical receivers, and does not require direct alignment of the transmitter and the receiver, as shown in Fig 2.1 (b). Nondirected LOS configuration can offer a broad signal coverage area. They can overcome signal blocking problem by receiving reflected signals from surfaces of objects in the room. It is, therefore, considered as the most flexible configuration. However, the nondirected LOS link induces a high optical path loss and multipath interference, and therefore requires higher transmitted power. Also it brings about intersymbol interference (ISI) for the LOS signal, thus limiting the data rate.

In the diffuse configuration, a transmitter points directly towards the ceiling and gives off a wide light beam, as shown in Fig 2.1 (c). Similar to nondirected LOS configuration, this configuration does not require direct alignment of the transmitter and the receiver, and the optical signal can cover a broad area. However, the received signal suffers high path loss and severe multipath interference during the transmission in the diffuse link.

2.2 Model of Directed LOS Optical Channel

For indoor directed LOS and nondirected LOS schemes, there exists a directed LOS optical link between the LED and the optical receiver. In this LOS optical link, the LED is the light source, and the photodetector is used to collect optical signal and converts the optical signal to photocurrent. For the light source, assuming that the LED lighting has a Lambertian radiation pattern, the distribution of radiation intensity $R(\phi)$ is given by [10]

$$R(\phi) = \begin{cases} \frac{m+1}{2\pi r^2} \cos^m(\phi), & 0 \leq \phi \leq \pi/2 \\ 0, & \phi > \pi/2 \end{cases} \quad (2.1)$$

where m is the Lambertian order which is given by $m = -\ln 2 / \cos(\phi_{1/2})$, $\phi_{1/2}$ is the half power angle of the transmitter, ϕ is the angle of irradiance with respect to the transmitter axis, and r is the distance between a LED and a receiver.

For the receiver, assuming the photodetector has an active area A , and the optical signal impinges on the detector at the angle Ψ , the effective collecting area of the detector is given by

$$A_{eff}(\Psi) = \begin{cases} A \cos(\Psi), & 0 \leq \Psi \leq \pi/2 \\ 0, & \Psi > \pi/2 \end{cases} \quad (2.2)$$

In order to increase overall effective collecting area, the non-imaging concentrator is applied in the receiver. The gain of the concentrator $g(\Psi)$ is given by [19]

$$g(\Psi) = \begin{cases} \frac{n_c}{\sin^2 \Psi_c}, & 0 \leq \Psi \leq \Psi_c \\ 0, & \Psi > \Psi_c \end{cases} \quad (2.3)$$

where n_c is the refractive index, and Ψ_c is the field-of-view (FoV) of concentrator.

Then the channel DC gain of the LOS optical link from the LED to the photodetector can be model as [19][20]

$$H(0) = \begin{cases} \frac{m+1}{2\pi r^2} A \cos^m(\phi) T_s(\psi) g(\psi) \cos(\psi), & 0 \leq \psi \leq \Psi_c \\ 0, & \psi > \Psi_c \end{cases} \quad (2.4)$$

where Ψ is the angle of incidence with respect to the receiver axis, $T_s(\psi)$ is the gain of the optical filter.

The average transmitted optical power of light emitted from the LED is P_t , which is given by

$$P_t = \lim_{T \rightarrow \infty} \frac{1}{2T} \int_{-T}^T X(t) dt \quad (2.5)$$

where $X(t)$ is the instantaneous transmitted optical power. Then, the average received optical power P_r that photodetector collects is given by

$$P_r = H(0)P_t \quad (2.6)$$

2.3 Model of Nondirected LOS Optical Channel

For indoor nondirected LOS and diffuse schemes, there exists nondirected LOS optical channel between the LED and the optical receiver. This channel is affected by many factors, such as the room dimension, the arrangement of walls and objects in the room, the reflectivity of the walls, ceiling, and the surfaces of the objects in the room [10][21][22]. Therefore, it is really difficult to accurately characterize this kind of channel, and to predict the related path loss between the LED and the receiver. Previously,

researchers did a lot of research addressing this problem, and tried to accurately characterize nondirected LOS optical channel [21][22][23].

Here, we consider reflections from the walls, which is a relatively simple case. For the receiver, the average received optical power is given by

$$P_r = \sum^{LEDs} \left\{ P_t H_d(0) + \int_{walls} P_t dH_{ref}(0) \right\} \quad (2.7)$$

where $H_d(0)$ is the channel DC gain of directed path, and $H_{ref}(0)$ represents reflected paths. Since the first reflection from the wall has largest effect on the LOS optical signal, here we consider the channel DC gain of the first reflection, which is given by

$$dH_{ref}(0) = \begin{cases} \frac{(m+1)A}{2\pi^2 D_1^2 D_2^2} \rho dA_{wall} \cos^m(\varphi) \cos(\alpha) \cos(\beta) T_s(\psi) g(\psi) \cos(\psi), & 0 \leq \psi \leq \Psi_c \\ 0, & \psi > \Psi_c \end{cases} \quad (2.8)$$

where D_1 is the distance between the LED and one reflective point on the wall, D_2 is the distance between the reflective point and the receiver, A is the area of the detector, ρ is the reflectance factor, dA_{wall} is the small reflective area in the wall, φ is the angle of irradiance with respect to the LED axis, α is the angle of incidence to a reflective point, β is the angle of irradiance to the receiver, and ψ is the angle of incidence as shown in Figure 2.2.

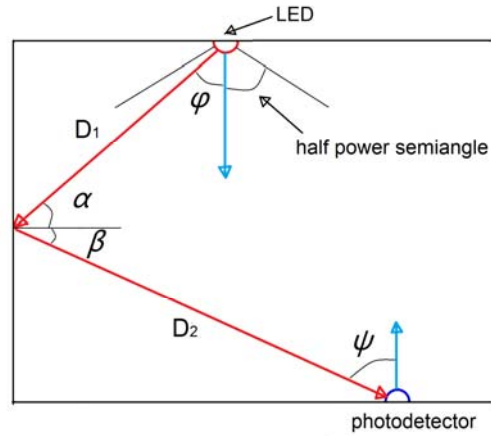


Figure 2.2: The first reflection of the nondirected LOS optical link.

Figure 2.3 shows the distribution of received optical power with first reflection [12]. The received optical power is -2.8 to 4.2 dBm for all the points in the room and the average received power is 2.5 dBm [12].

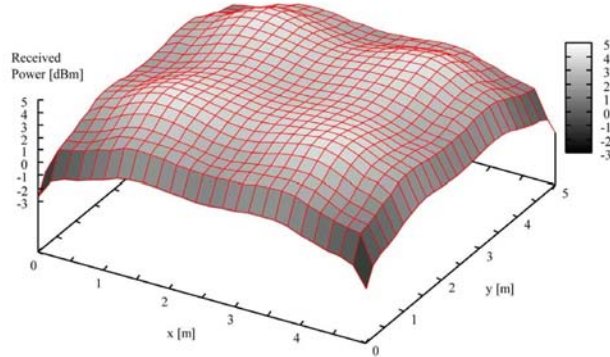


Figure 2.3: Distribution of received optical power with reflection [12].

2.4. Signal-to-noise Ratio Analysis

In this section, we will analyze the electrical signal-to-noise ratio (SNR), that is, the SNR of the photocurrent generated by the detector. In optical channels, the quality of

transmission is typically dominated by shot noise [24]. The shot noises mainly consist of shot noise caused by signals and shot noise induced by intense ambient light. Also we need to consider the effect of thermal noise. We assume that the noises as independent additive white Gaussian noises (AWGN) [12]. The received electrical power S and the electrical SNR are given by [12]

$$S = R^2 P_{rSignal}^2 \quad (2.9)$$

$$SNR = S / N \quad (2.10)$$

where R is the detector responsivity, N is the variances of all noises and interferences induced by the optical channel, and average received power of optical signal $P_{rSignal}$ is

$$P_{rSignal} = \int_0^T \left(\sum_{i=1}^{LEDS} h_i(t) \otimes X(t) \right) dt \quad (2.11)$$

where $X(t)$ represents the instantaneous transmitted optical power of each LED, $h_i(t)$ is the channel response for the link between each LED and the detector.

If there is no or little intersymbol interference (ISI) incurred by the optical channel, we could neglect the effect of ISI interference, and just consider the effect of the shot noise and thermal noise. Then the variance N is sum of the variances of shot noise and thermal noise, which is given by [10]

$$N = \sigma_{shot}^2 + \sigma_{thermal}^2 \quad (2.12)$$

where the shot noise variance is given by

$$\sigma_{shot}^2 = 2qRP_{rSignal}B + 2qI_{bg}I_2B \quad (2.13)$$

where q is the electronic charge, I_{bg} is background current, I_2 is the noise bandwidth factors, B is equivalent noise bandwidth. The thermal noise variance is the sum feedback-resistor noise variance and FET channel noise variance, which is given by

$$\sigma_{thermal}^2 = \frac{8\pi k T_K}{G} C_{pd} A I_2 B^2 + \frac{16\pi^2 k T_K \Gamma}{g_m} C_{pd}^2 A^2 I_3 B^3 \quad (2.14)$$

where k is Boltzmann constant, T_K is absolute temperature, G is the open-loop voltage gain, C_{pd} is the fixed capacitance of detector per unit area, Γ is the FET channel noise factor, and g_m is the FET transconductance.

If the ISI induced by multipath cannot be neglected, the variance N is given by [12]

$$N = \sigma_{shot}^2 + \sigma_{thermal}^2 + R^2 P_{rISI}^2 \quad (2.15)$$

where the average received power of intersymbol interference P_{rISI} is given by

$$P_{rISI} = \int_T \left(\sum_{i=1}^{\infty} h_i(t) \otimes X(t) \right) dt \quad (2.16)$$

From above analysis, we can see that the received electrical power of the detector is proportional to the square of the detector area, and the shot noise variance is proportional to the area of the detector. Hence, if the shot noise is the dominant noise, the electrical SNR is proportional to the area of the detector. According to information theory, as the SNR increases, the channel capacity also increases. Therefore, in order to obtain high SNR, the optical receiver should use large-area detector. However, as the detector area increases, its capacitance also increases. The increased capacitance has a limiting effect

on the receiving bandwidth of the detector, thus the channel capacity. This is in conflict with the increased bandwidth required by power efficient modulation schemes. Therefore, in order to obtain high receiving bandwidth of the receiver, we should adopt small-area detector in the optical receiver. During designing the VLC system, we should consider a trade-off between the electrical SNR and the receiving bandwidth of the receiver.

2.5 Discussion on Electrical SNR

In Komine's paper [12], the author defined the signal power S is

$$S = \gamma^2 P_{rSignal}^2 \quad (2.17)$$

where γ is detector responsivity and is same as R in (2.9), and

$$P_{rSignal} = \int_0^T [X(t) \otimes h(t)] dt \quad (2.18)$$

Therefore,

$$S = \gamma^2 P_{rSignal}^2 = \gamma^2 \left(\int_0^T [X(t) \otimes h(t)] dt \right)^2 \quad (2.19)$$

However, the author didn't denote what the signal S represents. According to other references [19], we can derive that the signal is the received electrical current, and S is the averaged received electrical signal power. In Komine's paper [12] and other references [10][19], the authors define the instantaneous received electrical current is

$$Y(t) = \gamma X(t) \otimes h(t) + N(t) \quad (2.20)$$

where $Y(t)$ is the received electrical current, $X(t)$ is the instantaneous transmitted optical power. Hence, according to equation (2.17) and the definition of signal power, the signal power S can be derived as

$$\begin{aligned}
S &= \frac{1}{T} \int_0^T [\gamma X(t) \otimes h(t)]^2 dt \\
&= \gamma^2 \frac{1}{T} \int_0^T [X(t) \otimes h(t)]^2 dt
\end{aligned} \tag{2.21}$$

Obviously, the result of equation (2.21) is not equal to that of equation (2.20).

Through analysis, we can find that since $X(t)$ is the instantaneous transmitted optical power, $X(t) \otimes h(t)$ is the instantaneous received optical signal power. Therefore, $P_{rSignal}$ defined in equation (2.18) represents the received “energy” over the time span $[0, T]$ rather than the received “power”. Here, we should define $P_{rSignal}$ as

$$P_{rSignal} = \frac{1}{T} \int_0^T [X(t) \otimes h(t)] dt \tag{2.22}$$

2.6 Conclusion

In this chapter, we have a systematic investigation of the three possible configurations of indoor VLC links, and evaluate the directed light-of-sight (LOS) optical channel and the nondirected LOS optical channel model. Then we investigate the electrical SNR for VLC channels. Finally, we provide closed-form derivations to clarify some confusion on the electrical SNR in the literature, and provide a better equation for the average received optical signal power.

Chapter 3

Indoor Localization Based on VLC

Indoor localization based on VLC is a novel localization technology with high positioning performance. In this chapter, we first illustrate and analyze VLC system using IM/DD, which is the basis for VLC based indoor localization. Then we investigate four possible localization methods applied in VLC based indoor localization, including time of arrival (TOA) methods, time difference of arrival (TDOA) methods, received signal strength (RSS) methods and angle of arrival (AOA) methods, and analyze and compare the features of these localization methods. In the last section, we explore the DOP analysis for RSS-based localization using VLC. The DOP relates the localization error to the measurement error, which is an important and effective factor to evaluate the localization accuracy in GPS localization and AOA-based localization. But few works have been found to focus on DOP analysis for RSS-based indoor localization using VLC. We establish the relationship between positional DOP (PDOP) and localization errors for RSS-based indoor localization using VLC, then use PDOP to analyze two localization scenarios with different of LED grid patterns, quantize the effect of LED grid patterns on the position error of the mobile receiver, and present the simulation results.

3.1 VLC System using IM/DD

The diagram of VLC system using IM/DD is shown in Figure 3.1 [10]. For the transmitter, the modulation signal $m(t)$ directly modulates the drive current of the LED, which in turn varies the instantaneous optical power radiated from the LED. For the

receiver, the output signal of the photodetector is photocurrent. This photocurrent is proportional to the instantaneous received optical power incident on the photodetector, which is given by [10][12]

$$y(t) = Rx(t) \otimes h(t) + n(t) \quad (3.1)$$

where $y(t)$ is the received photocurrent, R is the detector responsivity, $x(t)$ represents the instantaneous optical power of radiated from the LED, $h(t)$ is the impulse response of the channel, $n(t)$ represents the AWGN, and the symbol \otimes denotes convolution. The channel model of VLC system using IM/DD is shown in Figure 3.2.

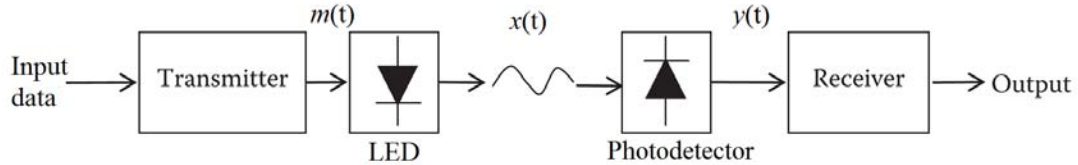


Figure 3.1: Illustrative diagram of VLC system using IM/DD.

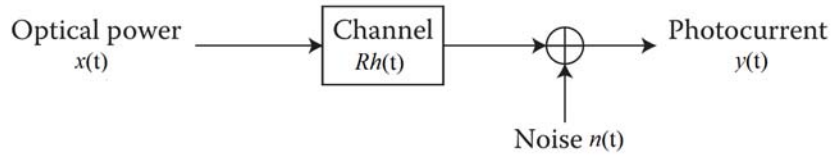


Figure 3.2: Channel model of VLC system using IM/DD.

3.2 Localization Methods for VLC Based Indoor Localization

The localization methods used for VLC based on indoor localization systems mainly include RSS methods [16][25][26], TOA methods [27], TDOA methods [28], and AOA methods [29]. Each positioning method has its own advantages and limitations.

TOA Methods

The basic idea of TOA methods is to accurately measure the propagation time of the direct line-of-sight (DLOS) signal from the transmitter to the receiver [4]. The distance from the LED to the target receiver is directly proportional to the propagation time of optical signals. In order to derive the location of the receiver using TOA measurements, signals from at least three LEDs must be obtained, as shown in Figure 3.3.

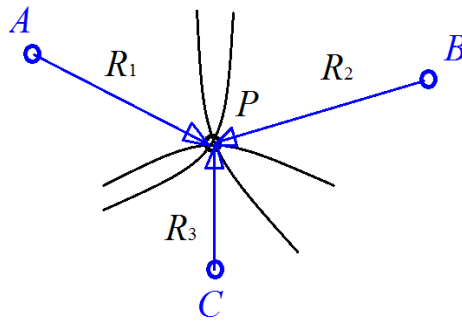


Figure 3.3: Localization based on TOA methods, where A , B and C are three LEDs, P is the target receiver, and R_1 , R_2 and R_3 represent the distance between A and P , B and P , and C and P respectively.

In general, TOA methods have several drawbacks. First, the propagation time of optical signals from the transmitter to the receiver is extremely short, and it is very difficult to measure this propagation time. Second, all transmitters and receivers in the positioning system have to be precisely synchronized. Third, a timestamp must be labeled

in the transmitted signal so that the target receivers can calculate the propagation time the signal has traveled. In TOA methods, even 1 ns measurement error in time can result in 0.3 m ranging error, and thus result in localization error. Therefore, TOA methods are not good choices for VLC based indoor localization.

TDOA Methods

In TDOA methods, the location of the target receiver is estimated based on the time differences of arrived signals transmitted from different LEDs, rather than the absolute arrival time of optical signals. Like TOA methods, the propagation time of optical signals is very short and could be not be long enough to be measured, and all transmitters and receivers in the TDOA based positioning system have to be precisely synchronized. Therefore, the TOA methods are not good choices for VLC based indoor localization.

RSS Methods

The RSS methods estimate the distance of the target receiver from some LEDs through measuring the attenuation of strength of optical signals emitted by LEDs, as shown in Figure 3.4. RSS methods calculate the signal path loss due to the propagation. Theoretical and empirical models are used to translate the difference between the transmitted signal strength and the received signal strength into a range estimate. RSS methods overcome the obvious limits of TOA and TDOA methods. However, we need to establish the accurate channel model and parameters to measure the path loss of the transmitted signal. In addition, as the indoor environment changes, the channel model and parameters may

also change. In general, compared with TOA and TDOA methods, the RSS methods are widely used VLC based indoor localization.

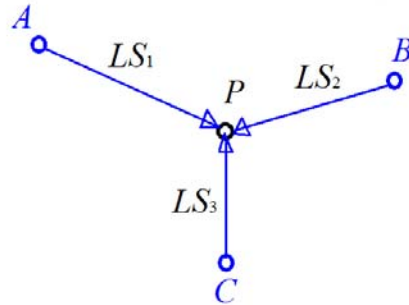


Figure 3.4: Localization based on RSS methods, where LS_1 , LS_2 , and LS_3 represent the measured path loss in three paths respectively.

AOA Methods

In AOA methods, the position of the target point can be estimated by the intersection of several pairs of angle direction lines [4]. In order to obtain 2D position estimation of the target, AOA methods require at least two LEDs with known positions, and two measured angles θ_1 and θ_2 to derive the 2D location of the target receiver P , as shown in Figure 3.5.

For 3D positioning, a 3D position can be estimated by as few as three LEDs.

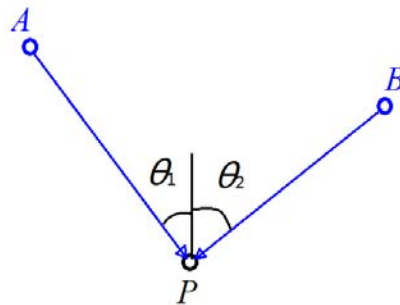


Figure 3.5: Localization based on AOA methods, where A, B and C are three LEDs, P is the target receiver, and θ_1 and θ_2 are two arrival angles.

This method doesn't require time synchronization between measuring units, and also overcomes the obvious limits of TOA and TDOA methods. However, for accurate positioning, the angle measurements need to be accurate. And the accuracy of angle measurement is limited by shadowing, multipath reflections from undirected directions, or the directivity of the measuring aperture [4]. In general, the AOA methods are also widely used VLC based indoor localization.

3.3 Dilution of Precision Analysis for RSS-based Localization using VLC

3.3.1 Formulation of Measurement Equation

RSS methods estimate the position of the mobile node based on the signal path loss due to propagation [11]. Empirical and theoretical models need to be established to relate signal path loss with the distance between transmitter and the receiver. In an LOS optical link, the channel DC gain can be model as the following equations [19][20]

$$H(0) = \begin{cases} \frac{m+1}{2\pi r^2} A \cos^m(\phi) T_s(\psi) g(\psi) \cos(\psi), & 0 \leq \psi \leq \Psi_c \\ 0, & \psi > \Psi_c \end{cases} \quad (3.2)$$

where m is the Lambertian order which is given by $m = -\ln 2 / \cos(\phi_{1/2})$, $\phi_{1/2}$ is half power angle of the transmitter, r is the distance between a LED lamp and a receiver, A is the area of the detector, ϕ is the angle of irradiance with respect to the transmitter axis, ψ is the angle of incidence with respect to the receiver axis, $T_s(\psi)$ is the gain of the

optical filter, $g(\psi)$ is the gain of the concentrator, Ψ_c is the field-of-view (FoV) of concentrator. The gain of the concentrator $g(\psi)$ is given by [19]

$$g(\psi) = \begin{cases} \frac{n_c}{\sin^2 \Psi_c}, & 0 \leq \psi \leq \Psi_c \\ 0, & \psi > \Psi_c \end{cases} \quad (3.3)$$

where n_c is the refractive index.

At the receiver side, the output signal of the photodetector (PD) is photocurrent. This photocurrent is proportional to the instantaneous received optical power incident on the PD, which is given by [12][19]

$$Y(t) = \gamma X(t) \otimes h(t) + N(t) \quad (3.4)$$

where $Y(t)$ is the received photocurrent, R is the detector responsivity, $X(t)$ represents the instantaneous optical power of the LED, $h(t)$ is the impulse response of the channel, $n(t)$ represents the AWGN and the symbol \otimes denotes convolution. When we employ on-off keying (OOK) modulation scheme, the difference between logical 0 and 1 in transmitted optical power P_{dt} is given as [30]

$$P_{dt} = \eta_{ook} P_{LED} \quad (3.5)$$

where η_{ook} is modulation depth, P_{LED} is the optical power emitted from LED lamp without modulation. At the receiver side, the difference in optical power between logical 0 and 1 is given by

$$P_{dr} = H(0)P_{dt} = H(0)\eta_{ook}P_{LED} \quad (3.6)$$

Based on equation (5), the measurement equation can be derived as follows [30][31]

$$g = RH(0)\eta_{\text{ook}}P_{\text{LED}} + n \quad (3.7)$$

where g is the photocurrent, and n is AWGN. When the angle of incidence is less than the FoV, the measurement equation can be written as

$$\begin{aligned} g &= \frac{R\eta_{\text{ook}}P_{\text{LED}}(m+1)}{2\pi r^2} A \cos^m(\phi) T_s(\psi) g(\psi) \cos(\psi) + n \\ &= \frac{k}{r^2} + n \end{aligned} \quad (3.8)$$

where k is given by

$$k = \frac{m+1}{2\pi} R\eta_{\text{ook}}P_{\text{LED}} A \cos^m(\phi) T_s(\psi) g(\psi) \cos(\psi) \quad (3.9)$$

3.3.2 DOP for RSS-Based Localization

DOP relates the position error with the measurement error. Previously, several DOP factors were established for GPS, such as Horizontal DOP (HDOP), Vertical DOP (VDOP), Positional DOP (PDOP), Time DOP (TDOP), and Geometric DOP (GDOP) [8]. These DOP factors are defined as the ratio of the statistical value of position errors to standard deviation (SD) of measurement errors. In this paper, we focus on PDOP, which is defined as

$$\text{PDOP} = \sqrt{\sigma_x^2 + \sigma_y^2 + \sigma_z^2} / \sigma_{\text{URE}} \quad (3.10)$$

Based on the measurement equation provided in section II, here we deduce PDOP for RSS-based localization using VLC. Considering m LEDs and one receiver in the localization scenario, the measurement equation for i th LED is given by

$$g_i = \frac{k_i}{r_i^2} + n_i \quad (3.11)$$

where r_i is the distance between the i th LED and the receiver, which is given by

$$r_i = \sqrt{(x_i - x)^2 + (y_i - y)^2 + (z_i - z)^2} \quad (3.12)$$

where (x_i, y_i, z_i) denotes the coordinate of i th LED in three-dimensional (3D) space, and (x, y, z) denotes the coordinate of the receiver in 3D space.

Firstly, we assume that there is no measurement noise (error) n_i , then the equation (10) can be linearized at the approximate coordinate of the receiver $(\hat{x}, \hat{y}, \hat{z})$ using Taylor expansion as follows

$$g_i = \hat{g}_i + a_{xi}\Delta x + a_{yi}\Delta y + a_{zi}\Delta z \quad (3.13)$$

where

$$\begin{aligned} \Delta x &= x - \hat{x}, \quad \Delta y = y - \hat{y}, \quad \Delta z = z - \hat{z} \\ \hat{g}_i &= \frac{k_i}{\hat{r}_i^2} \\ \hat{r}_i &= \sqrt{(x_i - \hat{x})^2 + (y_i - \hat{y})^2 + (z_i - \hat{z})^2} \\ a_{xi} &= \left. \frac{\partial g_i(x, y, z)}{\partial x} \right|_{(\hat{x}, \hat{y}, \hat{z})} = \frac{2k_i(x_i - \hat{x})}{\hat{r}_i^4} \\ a_{yi} &= \left. \frac{\partial g_i(x, y, z)}{\partial y} \right|_{(\hat{x}, \hat{y}, \hat{z})} = \frac{2k_i(y_i - \hat{y})}{\hat{r}_i^4} \\ a_{zi} &= \left. \frac{\partial g_i(x, y, z)}{\partial z} \right|_{(\hat{x}, \hat{y}, \hat{z})} = \frac{2k_i(z_i - \hat{z})}{\hat{r}_i^4} \end{aligned} \quad (3.14)$$

For $i = 1, 2, \dots, m$, the above linear equation can be written in a matrix form as

$$\Delta \mathbf{g} = \mathbf{H} \Delta \mathbf{x} \quad (3.15)$$

where

$$\Delta \mathbf{g} = \begin{pmatrix} g_1 - \hat{g}_1 \\ g_2 - \hat{g}_2 \\ \vdots \\ g_m - \hat{g}_m \end{pmatrix}, \quad \mathbf{H} = \begin{pmatrix} a_{x1} & a_{y1} & a_{z1} \\ a_{x2} & a_{y2} & a_{z2} \\ \vdots & \vdots & \vdots \\ a_{xm} & a_{ym} & a_{zm} \end{pmatrix}, \quad \Delta \mathbf{x} = \begin{pmatrix} \Delta x \\ \Delta y \\ \Delta z \end{pmatrix} \quad (3.16)$$

Using least square estimation, we can obtain the estimation of $\Delta \mathbf{x}$ from the following equation

$$\Delta \mathbf{x} = (\mathbf{H}^T \mathbf{H})^{-1} \mathbf{H}^T \Delta \mathbf{g} \quad (3.17)$$

Here, we assume \mathbf{H} is a nonsingular matrix. Therefore, $\mathbf{H}^T \mathbf{H}$ is a nonsingular and positive definite matrix.

When the measurement noise is taken into consideration, we have

$$\Delta \mathbf{x} + \mathbf{dx} = (\mathbf{H}^T \mathbf{H})^{-1} \mathbf{H}^T (\Delta \mathbf{g} + \mathbf{n}) \quad (3.18)$$

where \mathbf{n} is the measurement noise vector, and $\mathbf{n} = (n_1, n_2, \dots, n_m)^T$, \mathbf{dx} is the position error vector, and $\mathbf{dx} = (dx, dy, dz)^T$, here all the n_i are independent and identically distributed (i.i.d.) random variables, and each n_i is subject to zero mean Gaussian distribution. Therefore each dx_i is also subject to zero mean Gaussian distribution. Then we can obtain the covariance of position error vector \mathbf{dx} and covariance of measurement noise vector \mathbf{n} as

$$\begin{aligned} \text{cov}(\mathbf{dx}) &= E[\mathbf{dx} \mathbf{dx}^T] \\ &= E[(\mathbf{H}^T \mathbf{H})^{-1} \mathbf{H}^T \mathbf{nn}^T \mathbf{H} (\mathbf{H}^T \mathbf{H})^{-1}] \\ &= (\mathbf{H}^T \mathbf{H})^{-1} E[\mathbf{nn}^T] \end{aligned} \quad (3.19)$$

Since all the measurement noise n_i are independent and identically distributed, we have

$$E[n_i n_j] = \begin{cases} \sigma_n^2, & \text{if } i = j \\ 0, & \text{if } i \neq j \end{cases}, \quad i, j = 1, 2, \dots, m \quad (3.20)$$

where σ_n^2 is the variance of the measurement noise. Therefore, the covariance of position error vector \mathbf{dx} can be written as

$$\begin{aligned}\text{cov}(\mathbf{dx}) &= (\mathbf{H}^T \mathbf{H})^{-1} \mathbf{I}_{m \times m} \sigma_n^2 \\ &= (\mathbf{H}^T \mathbf{H})^{-1} \sigma_n^2\end{aligned}\quad (3.21)$$

Considering each element of $\text{cov}(\mathbf{dx})$, $\text{cov}(\mathbf{dx})$ can also be written as

$$\text{cov}(\mathbf{dx}) = \begin{pmatrix} \sigma_x^2 & \sigma_{xy}^2 & \sigma_{xz}^2 \\ \sigma_{xy}^2 & \sigma_y^2 & \sigma_{yz}^2 \\ \sigma_{xz}^2 & \sigma_{yz}^2 & \sigma_z^2 \end{pmatrix}\quad (3.22)$$

Therefore, the standard deviation of the position error can be derived as

$$\sqrt{\sigma_x^2 + \sigma_y^2 + \sigma_z^2} = \sqrt{\text{Tr}(\mathbf{H}^T \mathbf{H})^{-1}} \sigma_n\quad (3.23)$$

where σ_x^2 , σ_y^2 and σ_z^2 are the variance of position error in x dimension, y dimension and z dimension respectively, and $\text{Tr}(\bullet)$ represents the trace operation. Therefore, the expression of PDOP for the RSS-based positioning system is given by

$$\text{PDOP} = \sqrt{\text{Tr}(\mathbf{H}^T \mathbf{H})^{-1}}\quad (3.24)$$

3.3.3 Simulation Results

We consider two usual indoor localization scenarios using VLC. In scenario 1, the room dimension $L \times W \times H$ is $6 \times 6 \times 6 \text{ m}^3$, and four LED lamps are located at the four corners of the ceiling respectively, as shown in Fig. 3.6. The position of four LED lamps in scenario 1 are denoted by A(0, 0, 6), B(6, 0, 6), C(0, 6, 6), and C(6, 6, 6). In scenario 2, the room dimension $L \times W \times H$ is still $6 \times 6 \times 6 \text{ m}^3$, and four LED lamps are located in the central area of the ceiling, as shown in Fig. 3.8. The positions of four LED lamps in scenario 2 are

denoted by A(2, 2, 6), B(4, 2, 6), C(0, 6, 6), and C(6, 6, 6). The simulation parameters for LED and photo-detector (PD) are provided in Table 1 [30].

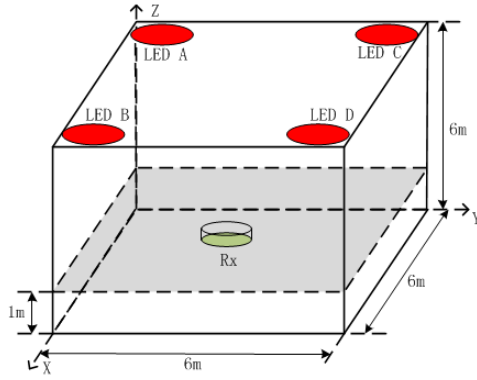


Figure 3.6: Indoor localization scenario 1

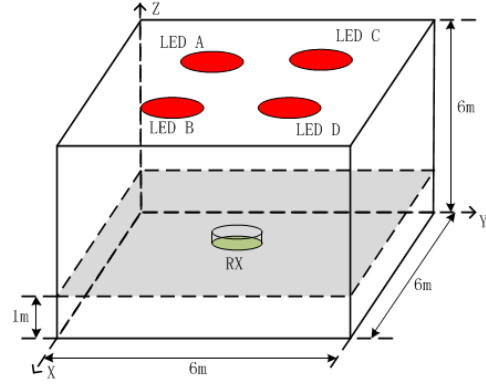


Figure 3.7: Indoor localization scenario 2

Parameters	Value
Power of Led without modulation (P_{LED})	16 W
Modulation bandwidth (W_B)	640 KHz
Modulation depth (η_{OOK})	12.5 %
Field of view (Ψ_c)	70°
Physical area of photo-detector (A)	1.0 cm ²
Gain of optical filter ($T_s(\psi)$)	1.0
Refractive index of optical concentrator (n_c)	1.5
Optical/Electrical conversion efficiency (R)	0.54 A/W

Table 3.1: Simulation parameters for LED and photodetector

In each scenario, we choose 31×31 positioning nodes on the $Z=1$ plane with each node being 0.2 m apart from its neighboring nodes, as shown in Fig. 3.8 and Fig. 3.9. At each node, the receiver axis is parallel with Z axis. Then we calculate the PDOP value for each positioning node. The statistics of all the PDOP values calculated at all the 31×31 nodes are further analyzed. The maximum PDOP value, minimum PDOP value, standard deviation (SD), and mean PDOP value are provided in Table 3.2.

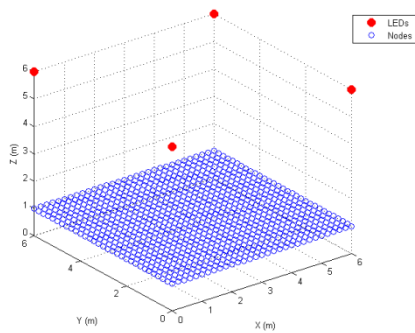


Figure 3.8: Positioning nodes in scenario 1

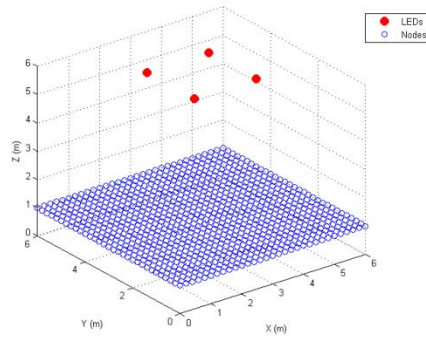


Figure 3.9: Positioning nodes in scenario 2

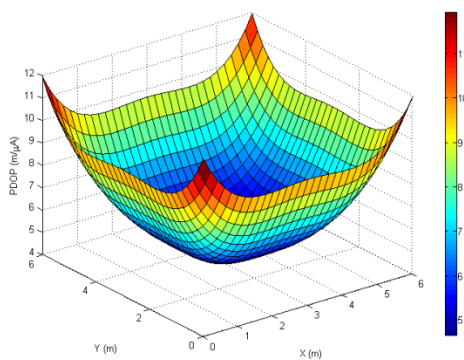


Figure 3.10: PDOP surface for scenario 1

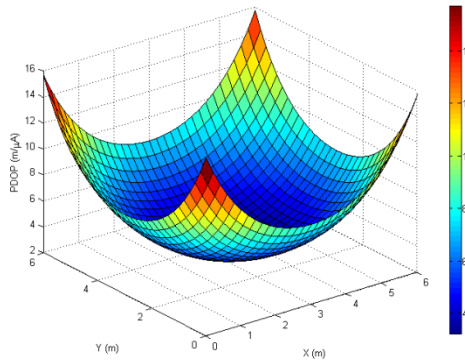


Figure 3.11: PDOP surface for scenario 2

	PDOP Value (m/μA)			
	maximum PDOP	minimum PDOP	SD	Mean
Scenario 1	11.9221	4.6479	1.7374	7.1011
Scenario 2	15.6918	3.2094	2.5350	6.4949

Table 3.2: PDOP value for RSS-based localization

	Node(s) with maximum PDOP	Node(s) with minimum PDOP
Scenario 1	Nodes at four corners	The central node
Scenario 2	Nodes at four corners	The central node

Table 3.3: Positions with maximum and minimum PDOP

Table 3.2 and Table 3.3 show that both mean PDOP and the minimum PDOP among all the positioning nodes in scenario 2 are smaller than those in scenario 1, which implies that we should place the LED lamps in the positions in scenario 2 if we want to achieve lower mean localization error, minimum localization error, and localization error around the center area. However, the maximum PDOP in scenario 1 is much smaller than that in scenario 2, which means we should we should place the LED lamps in the positions in scenario 1 if we want to obtain lower localization error around the four corners.

Chapter 4

Conclusion and Future Work

In this thesis, we build a clear and systematic investigation of the VLC channel models. We first investigate three possible configurations of indoor VLC links, and evaluate two widely used VLC channel models – the directed light-of-sight (LOS) optical channel and the nondirected LOS optical channel model. We next investigate the electrical SNR for VLC channels with intersymbol interference (ISI) and without ISI, and provide deduction and analysis to clarify some confusion on the electrical SNR in the literature.

We illustrate and analyze VLC system using IM/DD, which is the basis for VLC based indoor localization. Then we investigate, analyze and compare four possible localization methods applied in VLC based indoor localization, and point out that compared with TOA and TDOA methods, RSS and AOA methods are suitable for VLC based indoor localization. In the last, we establish the relationship between positional DOP (PDOP) and localization errors for RSS-based indoor localization using VLC, then use PDOP to analyze two localization scenarios with different of LED grid patterns, and quantize the effect of LED grid patterns on the position error of the mobile receiver. Simulation results show both mean PDOP and the minimum PDOP among all the positioning nodes in scenario 2 are smaller than those in scenario 1.

Future work will be focused on analysis of the effect of the angle of incidence, the angle of radiation, the dimension of the room on DOP factors including HDOP, VDOP and PDOP, and DOP analysis for more complex indoor environment.

References

- [1] N. Priyantha, A. Miu, H. Balakrishnan, and S. Teller, “The cricket compass for context-aware mobile applications,” 6th ACM Mobicom, July 2001, Rome, Italy.
- [2] P. Bahl and V. N. Padmanabhan, “RADAR: An in-building RF-based user location and tracking system,” in Proc. IEEE Infocom, 2000, Mar., vol. 2, pp. 775-784.
- [3] S. Gezici, Z. Tian, G. B. Giannakis, H. Kobayashi, A. F. Molisch, H. V. Poor, and Z. Sahinoglu, “Localization via ultra-wideband radios: A look at positioning aspects for future sensor networks,” IEEE Signal Process. Mag., vol. 22, no. 4, pp. 77-84, Jul. 2005.
- [4] H. Liu, H. Darabi, P. Banerjee, and J. Liu, “Survey of wireless indoor positioning techniques and systems,” IEEE Trans. Syst., Man, Cybernet., vol. 37, no. 6, Nov. 2007.
- [5] C. Starr, Biology: Concepts and Applications. Sixth Edition. Thomson Brooks/Cole, Belmont, California. 2005.
- [6] https://en.wikipedia.org/wiki/Electromagnetic_spectrum
- [7] O. Bouchet, M El Tabach, M Wolf, D C O’Brien et al., “Hybrid wireless optics (HWO): Building the next-generation home network,” 6th International Symposium on Communication Systems, Networks and Digital Signal Processing, CNSDSP, Graz, Austria, 2008, pp. 283–287.
- [8] M. A. Naboulsi, H. Sizun and F. Fornel, “Wavelength selection for the free space optical telecommunication technology,” Proc. SPIE 5465, Reliability of Optical Fiber Components, Devices, Systems, and Networks II, pp. 168–179, 2004.

- [9] M. Sze and K. K. Ng, *Physics of Semiconductor Devices*, 3rd ed. Hoboken, New Jersey: John Wiley & Sons Inc., 2007.
- [10] Z. Ghassemlooy, W. Popoola, and S. Rajbhandari, *Optical Wireless Communications: System and Channel Modelling With MATLAB*. CRC Press, 2012.
- [11] G. Reider, *Photonics: An Introduction*, Springer, 1st Edition, Boca Raton, FL, USA: CRC Press, 2012.
- [12] T. Komine and M. Nakagawa, "Fundamental analysis for visible-light communication system using LED lights," *IEEE Transactions on Consumer Electronics*, vol. 50, no. 1, pp. 100-107, Feb. 2004.
- [13] J. Senior, *Optical Fiber Communications Principles and Practice*, 3rd ed, Essex: Pearson Education Limited, 2009.
- [14] W. K. Pratt, *Laser Communication Systems*, 1st ed, New York: John Wiley & Sons Inc., 1969.
- [15] J. Lim, "Ubiquitous 3D positioning systems by led-based visible light communications," *IEEE Wireless Communications*, vol. 22, no. 2, pp. 80-85, Apr. 2015.
- [16] G. Prince and T.D.C. Little, "A Two Phase Hybrid RSS/AoA Algorithm for Indoor Device Localization using Visible Light," *Proc. IEEE Globecom Conference 2012*, Anaheim, CA, Dec 2012.

- [17] A. M. Street, P. N. Stavrinou, D. C. O'Brien and D. J. Edwards, "Indoor optical wireless systems—A review," *Optical and Quantum Electronics*, 29, pp. 349-378, 1997.
- [18] P. S. Peter, L. E. Philip, T. D. Kieran, R. W. David, M. Paul and W. David, "Optical wireless: A prognosis," *Proc. SPIE*, PA, USA, 1995, pp. 212-225.
- [19] J. M. Kahn and J. R. Barry, "Wireless infrared communications," *Proceedings of the IEEE*, vol. 85, no. 2, pp. 265-298, Feb. 1997.
- [20] J. R. Barry, *Wireless Infrared Communications*, Kluwer Academic Press, Boston, MA, 1994.
- [21] N. Hayasaka and T. Ito, "Channel modeling of nondirected wireless infrared indoor diffuse link," *Electronics and Communications in Japan*, 90, pp. 9-19, 2007.
- [22] J. B. Carruthers and J. M. Kahn, "Modeling of nondirected wireless Infrared channels," *IEEE Transaction on Communication*, 45, pp. 1260-1268, 1997.
- [23] V. Jungnickel, V. Pohl, S. Nonnig and C. Helmolt, "A physical model of the wireless infrared communication channel," *IEEE Journal on Selected Areas in Communications*, 20, pp. 631-640, 2002.
- [24] M. Yoshino, S. Haruyama and M. Nakagawa, "High-accuracy positioning system using visible LED lights and image sensor," 2008 IEEE Radio and Wireless Symposium, Orlando, FL, 2008, pp. 439-442.
- [25] M. Rahaim, G. B. Prince, and T. D. C. Little, "State estimation and motion tracking for spatially diverse VLC networks," in *Proc. 3rd IEEE Workshop on Optical Wireless Communications*, Anaheim, CA, pp. 1249-1253, Dec. 2012.

- [26] H. S. Kim, D. R. Kim, S. H. Yang, Y. H. Son and S. K. Han, "An Indoor Visible Light Communication Positioning System Using a RF Carrier Allocation Technique," *Journal of Lightwave Technology*, vol. 31, no. 1, pp. 134-144, Jan. 2013.
- [27] T. Q. Wang, Y. A. Sekercioglu, A. Neild, J. Armstrong, "Position Accuracy of Time-of arrival Based Ranging Using Visible Light With Application in Indoor Localization Systems", *Journal of Lightwave Technology*, pp. 3302-3308, Oct. 2013.
- [28] S.-Y. Jung, S. Hann, and C.-S Park, "TDOA-based optical wireless indoor localization using LED ceiling lamps," *IEEE Trans. Consum. Electron.*, vol. 57, no. 4, pp. 1592-1597, Nov. 2011.
- [29] S. H. Yang, H. S. Kim, Y. H. Son, S. K. Han, "Three-Dimensional Visible Light Indoor Localization Using AOA and RSS With Multiple Optical Receivers", *Journal of Lightware Tech.*, pp. 2480-2485, 2014.
- [30] W. Zhang, M. I. S. Chowdhury, and M. Kavehrad, "Asynchronous indoor Positioning System Based on Visible Light Communications," *Opt. Eng.*, vol. 53, no. 4, pp. 1-9, Apr. 2014.